

Chapter 6

Hygroelectricity: The Atmosphere as a Charge Reservoir

Contents

6.1	Water Vapor Sorption in Solids.....	65
6.1.1	Water Vapor Adsorption Isotherms.....	66
6.2	Charging Cellulose Under High Humidity	67
6.3	Charging Metals with Atmospheric Humidity.....	70
6.4	The Effect of Humidity on Surface Charge Patterns	72
6.4.1	Water Vapor Adsorption and Desorption Modifies Charge Patterns	72
6.4.2	Charge Build-Up on KFM Calibration Samples.....	77
6.4.3	Excess Charge Decay Through the Atmosphere.....	79
6.5	Flow Electrification: The Position of Water in the Triboelectric Series	82
6.6	Water Dropping from a Biased Needle.....	83
6.7	Spontaneous Electric-Bipolar Nature of Aerosols.....	86
6.8	Conclusion and Prospects	88
	References.....	89

6.1 Water Vapor Sorption in Solids

Water sorption and desorption are very important in nature, since the survival of any species largely depends on water availability. Wherever water is scarce, the atmospheric vapor becomes an important source of water. The success of a species in these places depends then on developing strategies for using condensed water or for adsorbing it from the air.

“Non-rainfall” water on soil is important in arid zones, where dew can be the sole source of water for plants. Dew formation and direct water vapor adsorption are

effective mechanisms for supplying water to the soil. Depending on surface temperature, water vapor adsorption is the only mechanism for water uptake by the soil [1].

Water vapor adsorption on solids is also a matter of great practical interest for many important products like pharmaceuticals, food, clothing and electronic ware whose production, durability and performance may be strongly affected by adsorbed water.

6.1.1 Water Vapor Adsorption Isotherms

Water vapor adsorption is known among practitioners as a broad, complex topic. Its difficulties are indeed expected, considering the relative contributions of various types of intermolecular interactions leading to the tendency of water molecules to cluster [2]. Another important factor is the pronounced amphoteric character of water that strongly contributes to its interactions with many solids.

An important feature is the size of water molecule that is smaller than the widely used N_2 . For this reason, it was used instead of nitrogen to determine the pore structure in solids many years ago, using BET isotherms and especially t -curves that yield the statistical thickness of water films. A main advantage is that many important adsorbents have a significant part of their pore systems inaccessible to nitrogen but accessible to water vapor [3].

Other isotherms were used for different systems. For instance the Dubinin-Radushkevitch equation [4] has been widely used to quantitatively describe the adsorption of gases and vapors by microporous sorbents, as for instance carbon. This equation is based on the assumption that pore-filling is the relevant mechanism, rather than multilayer surface coverage. In one recent work, the modified Dubinin–Astakhov equation was used in the cases of activated carbon and alumina while the Langmuir equation was used in the case of carbon impregnated with $CaCl_2$, yielding good agreement with the experimental data [5].

Beyond isotherms, the structural properties of adsorbed water are by themselves a challenging topic. This is illustrated by a recent publication [6] on water vapor adsorption on single-wall nanotubes: water molecules form a thin (1–2 monolayers) adsorption layer created by lateral hydrogen bonds among molecules bound to the nanotube by van der Waals forces. The authors did not find evidence for charge transfer and the nanotubes coated with water are macroscopically hydrophobic. Following this paper and a large part of the literature on water vapor adsorption, electrostatic interactions do not play a role in water adsorption or desorption at the solid–gas interfaces. However, this role has now been demonstrated in many cases that are described in the following sections of this chapter.

6.2 Charging Cellulose Under High Humidity

Conventional wisdom says that electrostatic charge tends to disappear under high atmospheric humidity. For this reason, the results reported by Soares et al. [7] were rather surprising and they are among the first recorded evidence showing charge build-up under *high* humidity.

This work used a simple but well defined set-up that produced highly reproducible experimental results. Essentially, the positive electrostatic potential of an electrified acrylic sheet was measured under controlled relative humidity (RH) values, using a Kelvin electrostatic voltmeter. A sheet of filter paper that is essentially a cellulose film was then quickly introduced between the electrified solid and the electrode, while the Kelvin instrument readings were recorded, decaying toward zero. Then, the acrylic sheet was quickly withdrawn and the voltmeter readings became negative, showing that the paper had accumulated excess negative charge under the positive potential of the acrylic. The negative potential of the paper which was dissipated decayed again back to zero, following a curve symmetrical to that observed in the first step of the experiment, when the acrylic sheet was introduced. This is shown in detail in Fig. 6.1.

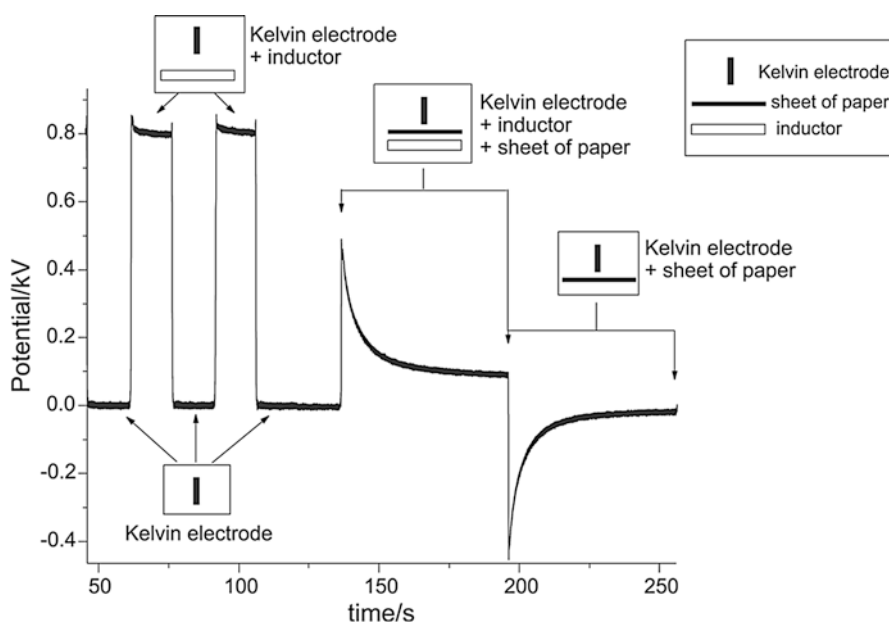


Fig. 6.1 Potential vs. time (at 10% RH and with one sheet of paper). The inductor was periodically introduced beneath the electrode during the experiment. The quasi-square waves to the left were recorded when the inductor was introduced and removed while the paper sample was withdrawn. The spikes in the central part show potential readings when the paper sample is positioned beneath the electrode. Positive potentials were observed when the inductor was introduced and near-zero or negative potentials were obtained while the inductor was withdrawn. Reprinted with permission from [7]

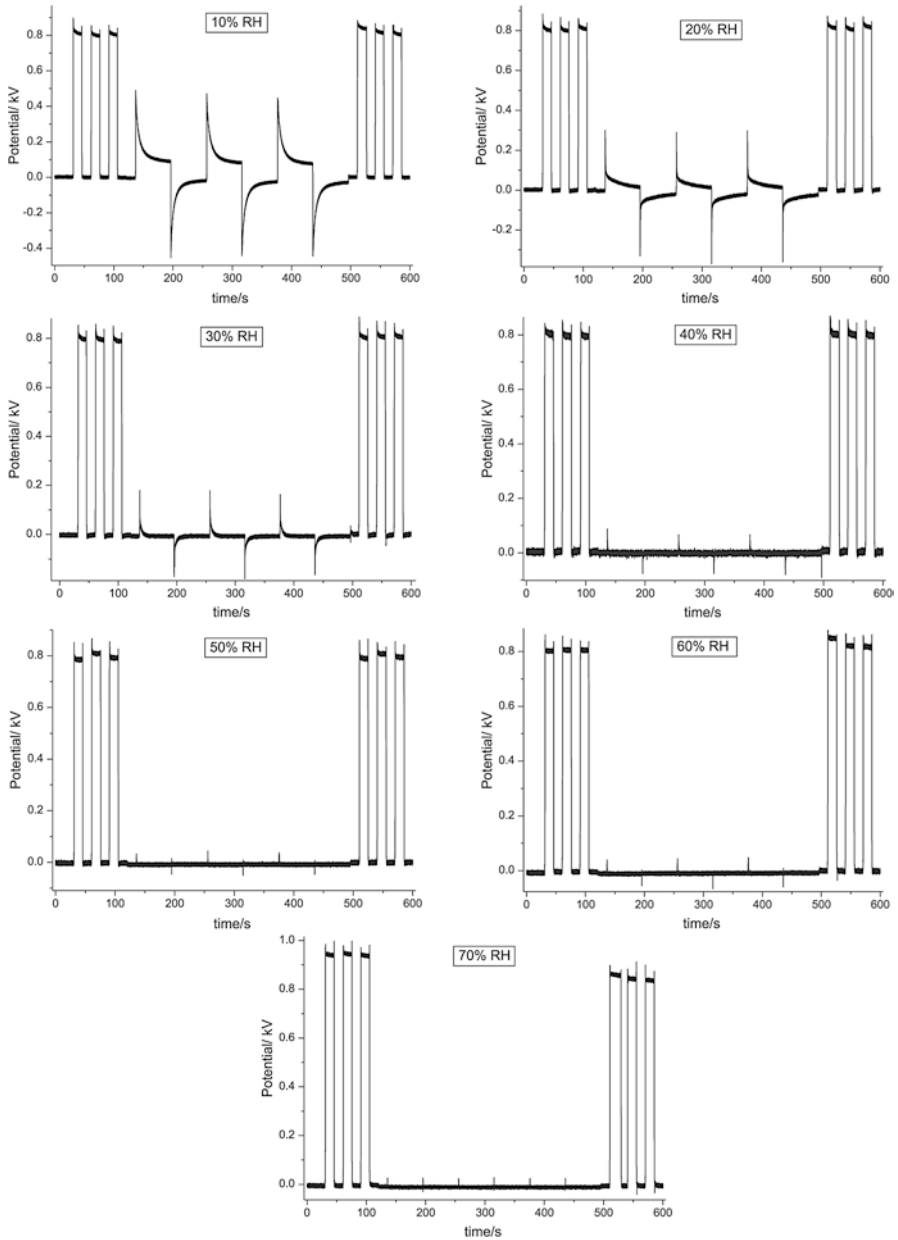


Fig. 6.2 Potential vs. time curves recorded for paper sheet under nitrogen, 10–70% relative humidity. Details are as in the legend of Fig. 6.1 Reprinted with permission from [7]

The effect of increasing relative humidity is shown in Fig. 6.2. Cellulose displays a significant shielding ability for DC and low-frequency AC fields, under RH equal or larger than 50%.

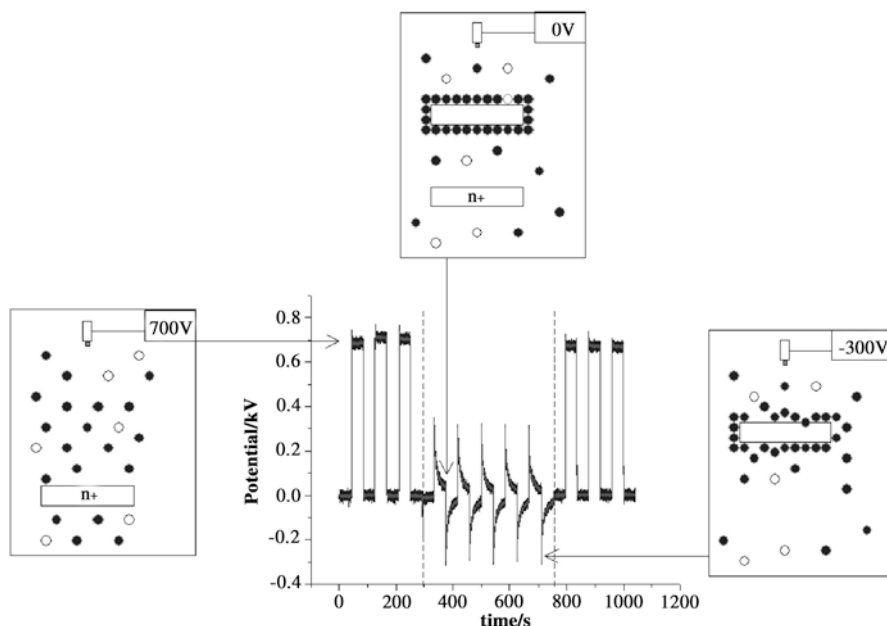


Fig. 6.3 Schematic representation of the mechanism proposed for the observed potential changes. *Left*: the poled inductor is introduced beneath the electrode that reads the potential created by all charges in the vicinity, both in the inductor as well as in the atmosphere. *Center*: the sample is introduced between the poled inductor and the electrode. The accumulation of charged water cluster ions in the sample surface leads to a decrease in the potential read by the electrode. *Right*: the poled inductor is withdrawn and the voltmeter reads a potential generated by the excess negative charge at the sample surface. *Black circles* are negative ion clusters and the *white circles* are positive charges. The potential vs. time plot in the center of the figure shows the points corresponding to the three states. Reprinted with permission from [7]

Figure 6.3 is a schematic representation of the main events in these experiments, showing how the accumulation of negative ions on cellulose under the positive potential of the charged acrylic sheet produces zero reading in the electrometer.

These results could not be explained using the usual induction models that are adequate for metals or semi-conductors, based on charge displacement across the insulator. They are also different from what would be expected if the shielding effect was solely based on water dipole orientation, because this is a much faster phenomenon with relaxation times in the microsecond range.

On the other hand, they are consistent with the hypothesis of sorption of atmospheric water on the insulator and its electrification, based on the effect of the applied *electric potential* on the *electrochemical potential* ($\mu_i = \mu_i^\circ + RT \ln a_i + zFV$). This produces excess concentrations of the ions formed by water adsorbed on cellulose, $H(H_2O)_n^+$ and $OH(H_2O)_n^-$.

This also helps to understand the nature of space charge associated with dielectrics in the presence of even minute amounts of water. Space charge is often mentioned but it is hardly identified with definite chemical species. These results led

thus to a new model for electrostatic charging of dielectrics, based on excess $\text{H}(\text{H}_2\text{O})_n^+$ and $\text{OH}(\text{H}_2\text{O})_n^-$ ions formed and trapped within the solid surface and bulk.

Estimates of the concentration of excess charge from potential measurements yield very low charge densities. For instance, in an experiment of charge induction in paper sheets [7], carried out at 10% RH, 500 V were detected at the electrode probe. The calculated charge concentration is 1×10^{-2} unit charge/ μm^3 , only. Concentration-wise this is low but it is significant, as far as the resulting voltage is concerned.

6.3 Charging Metals with Atmospheric Humidity

In 2010, Ducati et al. [8] showed that the exposure of isolated metal samples to water vapor leads to the deposition of excess charge on the metal, measured using a Faraday cup.

A typical set of results is in Fig. 6.4, showing how periodic change in relative humidity produces the accumulation of negative charge on chrome-plated brass tubing.

Fig. 6.4 RH, charge per area, and charge change rate vs. time plots for a chrome-plated-brass (CPB) tubing during dry-wet-dry N_2 cycles. Reprinted with permission from [8]

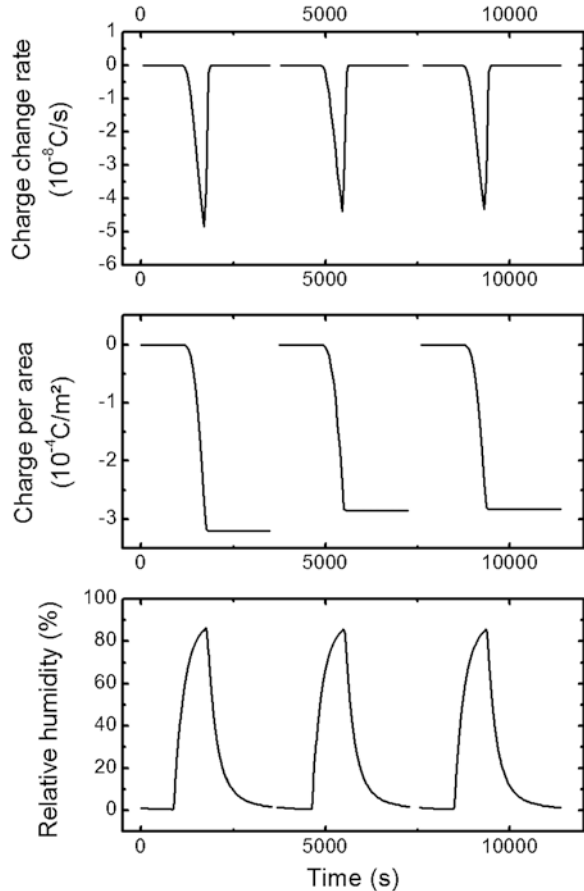
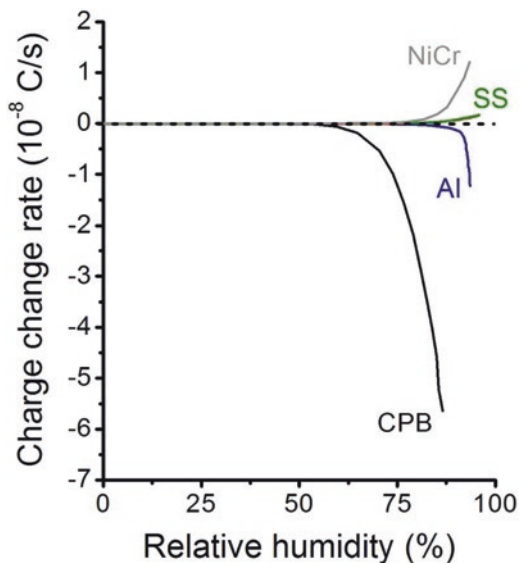


Fig. 6.5 Charge change rate dependence on increasing RH for NiCr, stainless steel (SS), aluminum (Al) and chrome-plated-brass (CPB). Rates for brass, copper, silicone-coated aluminum and stainless steel are negligible in the scale shown here. Reprinted with permission from [8]



Experiments like these were performed using many different metals and the accumulated results for aluminum, stainless steel, nichrome, brass, chrome-plated brass and copper are in Fig. 6.5. Copper and brass acquire little charge, nichrome and stainless steel become positive while aluminum and Cr-plated brass become negative.

CPB is not a usual laboratory material but it was important for the discovery of hygroelectricity, since it acquires higher charge than any other material tested so far. This kind of tubing was acquired by a student in the author's laboratory, who was in a hurry to build a Faraday cup and did not want to wait for delivery of the copper tubing. Instead, she found this tubing in a store selling building and home repair materials, and acquired it. If the student would build a more standard Faraday cup using copper metal, hygroelectricity would not have been discovered, probably.

Charging isolated metals within shielded and grounded containers without resorting to any source of electricity shows that the atmosphere can transfer charge to the metals. Thus, it is a charge reservoir for both positive and negative charge. Since the positive or negative current entering the otherwise electrically isolated metal is strongly dependent on the relative humidity, it is assigned to OH^- and H^+ ions transfer to gas–solid interfaces, producing net current. The electricity buildup dependence on humidity, or hygroelectricity, acts simultaneously but in opposition to the well-known charge dissipation due to the increase in surface conductance of solids under high humidity. Indeed, metal charging by adsorption of water vapor ions beats surface conductance.

The reason for obtaining positive or negative charge is assigned to specific adsorption on the metal surface or else, on the oxide layer coating the metal: if this adsorbs preferentially OH^- or H^+ , it will acquire excess negative or positive charge. This is represented in Fig. 6.6.

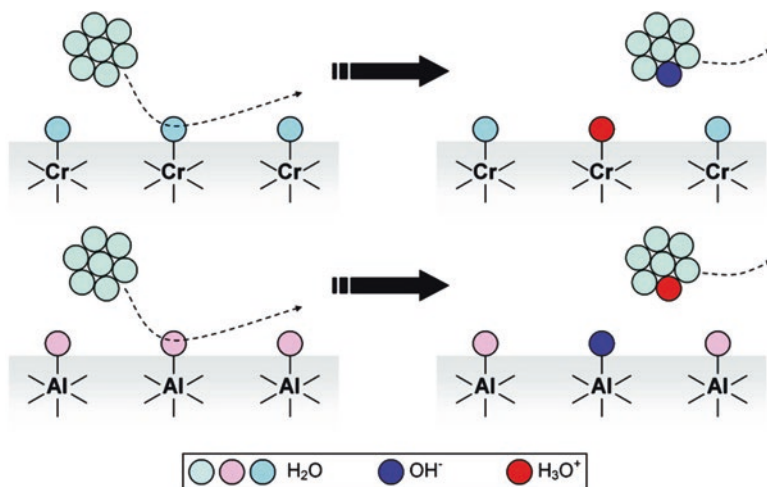


Fig. 6.6 Mechanism for charge transfer from the atmosphere to the metal surface. (*Top*) Formation of positive charge over a basic oxide. (*Bottom*) Formation of negative charge over an acidic oxide. Neutral water molecules are amphoteric, reacting differently with different oxides according to their acid–base properties. Reprinted with permission from [8]

This phenomenon holds the potential to produce power by scavenging electricity from the atmosphere. Hygroelectricity cells were built in the author’s group, combining aluminum as the negative electrode using stainless steel and carbon as the positive electrode. This is an asymmetric capacitor, self-charging to 0.7 V spontaneously under 80% RH. Unfortunately, repeated charge/discharge cycles of the capacitor are accompanied by aluminum oxidation, which is highly undesirable. Consequently, practical use of hygroelectricity as a way to scavenge energy from the ambient still depends on finding more durable materials. Nevertheless, a group in Indonesia concluded that “... Indonesia has the potential to harness hygroelectricity to solve the energy crisis and environmental issues” [9].

6.4 The Effect of Humidity on Surface Charge Patterns

6.4.1 Water Vapor Adsorption and Desorption Modifies Charge Patterns

The discovery of the effect of changing relative humidity on the excess charge in metals and cellulose came soon after the independent discovery of charge patterns in almost any dielectric particles and films that were examined by scanning probe electric microscopies. For this reason, Kelvin micrographs were acquired from different materials under high and low humidity, starting with films of non-crystalline silica and aluminum phosphate fine particles [10], followed by many other solids.

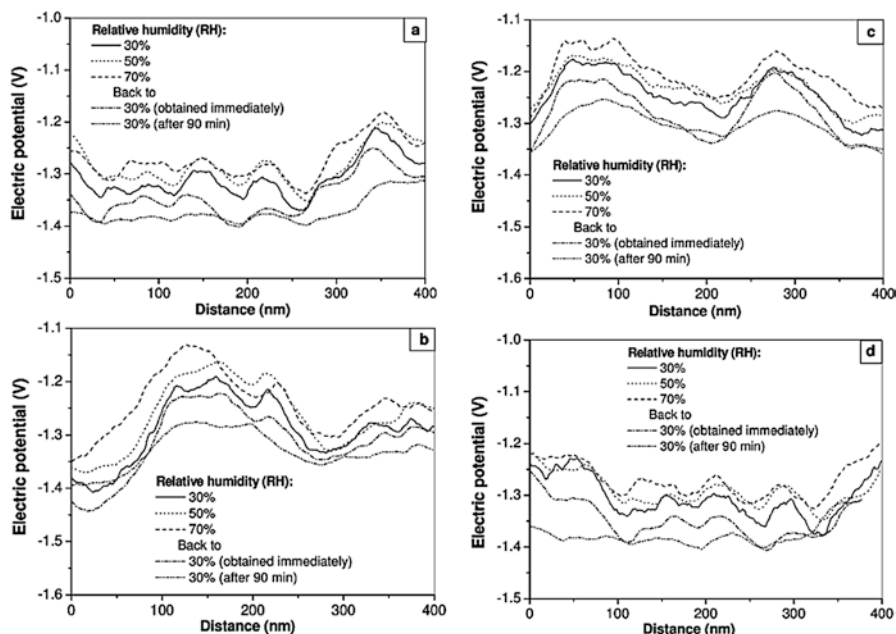


Fig. 6.7 Line-scans from the five consecutive KPM images from aluminum phosphate particles. Reprinted with permission from [10]

In every case that was examined, the electrostatic potential patterns change with the relative humidity, within an electrically shielded and grounded environment, as shown in Figs. 6.7 and 6.8, obtained for aluminum phosphate and Stöber silica nanoparticle films.

Moreover, the observed change is not uniform, across the samples. Potential adjacent to the particle surfaces is always negative and Fig. 6.9 shows potential gradients in excess of 10 MV/m, parallel to the film surfaces.

The examination of many other solids with known acid–base character [11] showed that the electrostatic potential at the surface of acidic solids becomes more negative under higher relative humidity (RH), while basic solids acquire a more positive potential at high RH, using the Kelvin method at the nano- and macroscales, see Table 6.1.

Images acquired in the Kelvin microscope under low and high humidity are in Fig. 6.10, together with the corresponding potential traces. Silica, iron oxide on iron and cellulose show parallel traces evidencing that the surface is uniform, concerning its acid–base character. On the other hand, aluminum oxide on metal is rather non-uniform. Moreover, changes on silica are highly reversible but on cellulose they are not.

Table 6.1 sums up the results obtained for nine solids. The average potential variations, ΔV for iron oxide on iron and calcium oxide are very large and the uniformity parameter $R = (\Delta V_m)2/(\Delta V)^2_m$ approaches unity for a few solids but it is only 0.4 for MgO, showing that this has a very non-uniform surface.

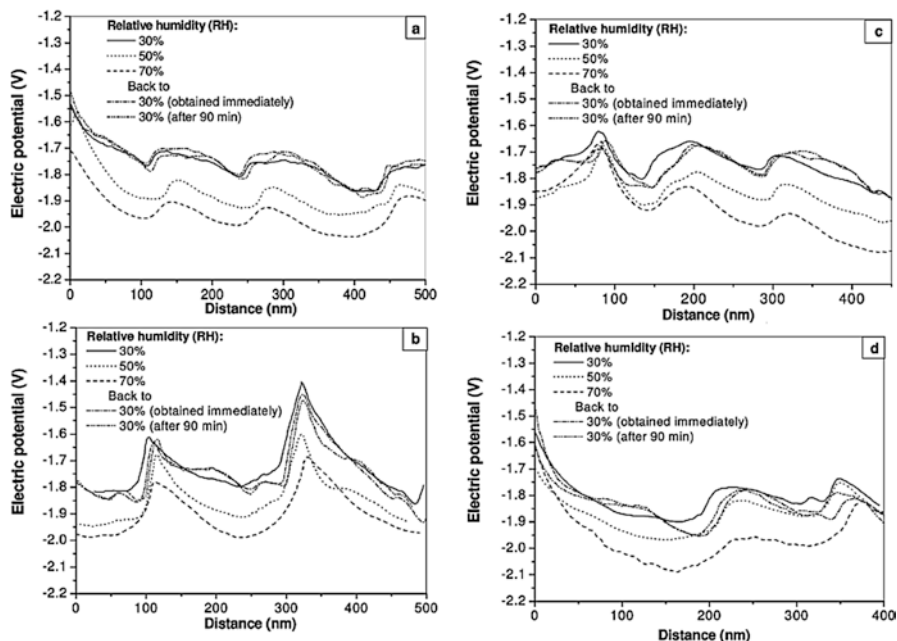


Fig. 6.8 Line-scans from the five consecutive KPM images from Stöber silica particles. Reprinted with permission from [10]

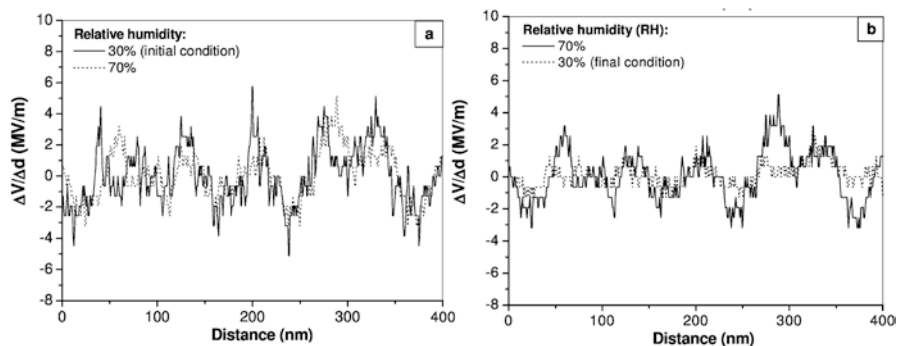


Fig. 6.9 Electric potential gradients calculated as a function of the sample position for Stöber silica particles after equilibrating for 90 min. (a) 30% RH (solid line, initial condition) and 70% RH (dot line). (b) 70% RH (solid line) and 30% RH (dot line, final condition). Reprinted with permission from [10]

This provided a basis for the selectivity of H^+ or OH^- adsorption from water vapor: acidic surfaces adsorb OH^- while basic surfaces adsorb H^+ . Thus, the key factor for predicting the effect of changing humidity on KFM microscopy is the Brønsted acid or base character of the solid under examination. Kelvin microscopy

Table 6.1 Average electrostatic potential variation (ΔV_m) and the mean square $(\Delta V_m)^2_m$ for the analytical solids, following an increase in humidity (from 30% RH to 70% RH) [11]

Compound	ΔV_m	$(\Delta V_m)^2$	$R = (\Delta V_m)^2 / (\Delta V_m)^2_m$	Assignment
Iron oxide	-0.464 ± 0.004	0.217 ± 0.004	0.99	Acid
Magnesium sulfate	-0.229 ± 0.008	0.063 ± 0.009	0.83	Acid ^a
Silica	-0.172 ± 0.015	0.033 ± 0.005	0.90	Acid ^b
Cellulose	-0.104 ± 0.007	0.011 ± 0.001	0.98	Acid
Aluminum oxide	-0.055 ± 0.016	0.004 ± 0.002	0.76	Acid ^a
Calcium oxide	$+1.657 \pm 0.115$	2.811 ± 0.335	0.98	Base ^b
Magnesium oxide ^c	$+0.195 \pm 0.062$	0.096 ± 0.021	0.40	Base ^a
Nickel oxide	$+0.060 \pm 0.017$	0.005 ± 0.002	0.72	Base
Aluminum phosphate	$+0.039 \pm 0.007$	0.002 ± 0.001	0.76	Base ^b

^aData taken from [12]^bData taken from [8]^c30–50% RH only. This cannot be measured at 70% RH because of excessive water absorption

under variable humidity also provides information on the spatial distribution of acid–base sites, which is currently inaccessible to any other technique.

These results enlarged the scope of Kelvin force microscopy (KFM) that was then identified as a powerful, sensitive, and convenient technique for the detection and characterization of acid and base sites on solid surfaces, including adsorbents and catalysts. It shows many positive characteristics:

1. The only reagent used is water vapor. Thanks to its amphoteric behavior, water detects both acidic and basic sites;
2. The activity of the reagent water vapor is easily changed by changing the relative humidity;
3. Detection sensitivity is very large, especially when compared to widespread surface analytical techniques, since it is based on charge and potential measurements;
4. Uniformity (or not) of acid – base sites is easily detected, with a spatial resolution in the 10–20 nm range;
5. Standard noncontact atomic force microscopy (AFM) micrographs are acquired simultaneously with Kelvin images, revealing concurrent changes in the solid morphology, if any;
6. Kelvin microscopes are currently commercially available from many suppliers as attachments to AFM instruments.

Many perspectives are now open to this technique, since measurements can be done on different time scales in the range of many minutes and up, allowing the acquisition of kinetic information. Moreover, the spatial resolution can probably be improved in very smooth surfaces, such as those in well-defined single crystals, using high-resolution Kelvin microscopy [13].

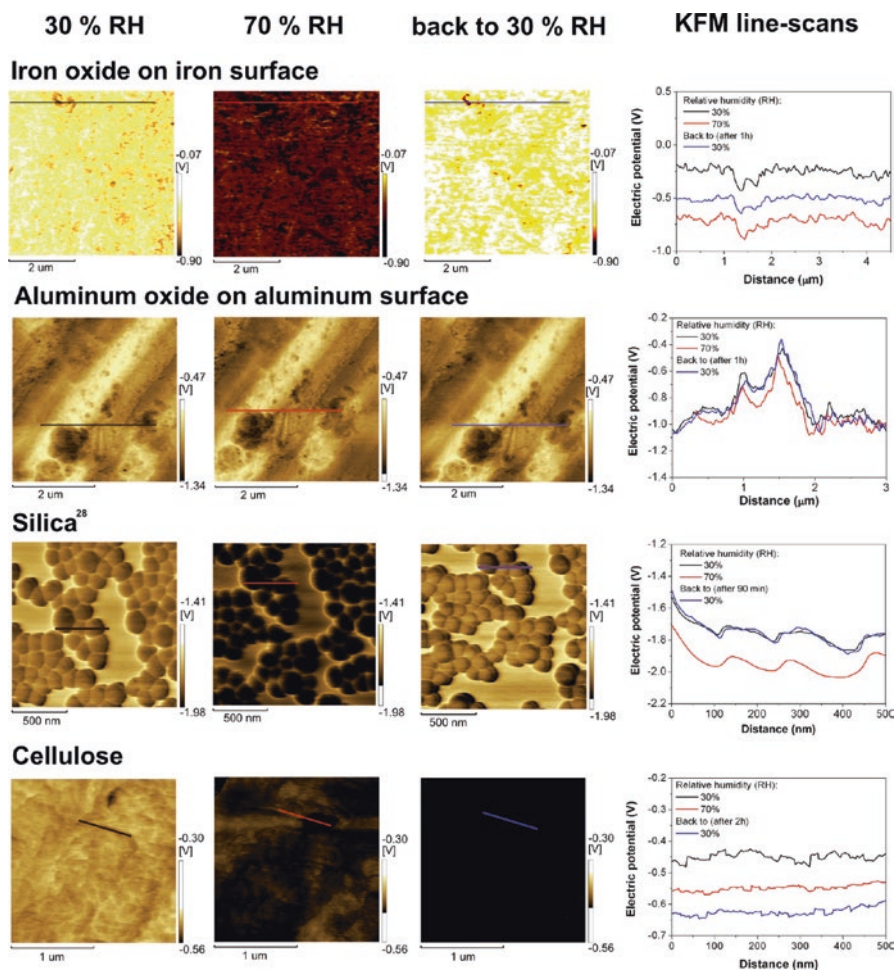


Fig. 6.10 KFM images and line-scans from the same area of iron oxide on metal, aluminum oxide on aluminum metal, silica and cellulose. Successive changes in the relative humidity (RH) were made prior to image acquisition, as indicated at the top of the figure. Darker areas are more negative than the brighter areas. The observed changes are at least partly reversible, except in the case of cellulose. Reprinted with permission from [11]

Many more additional parameters can be examined: sample temperature cycling effects, the presence of other gases [14] in the surrounding atmosphere (including hydrocarbons, alcohols, ammonia, pyridine, and CO_2), and the effect of pressure, within the limits defined by the available instrumentation.

To conclude, KFM that was initially designed to map electric potential holds an unmatched potential to advance knowledge on the acid – base behavior of solid surfaces, producing hitherto unavailable analytical information on important chemical systems.

6.4.2 Charge Build-Up on KFM Calibration Samples

Kelvin probe or Kelvin force microscopes (KFM) and other types of scanning probe instruments derived from the atomic force microscope have been playing a key role in the progress in discovering electrostatic patterns in surfaces in the last 20 years. This in turn led to radical revision of some widespread ideas that lacked strong experimental basis.

To make sure that the measurements made on a Kelvin microscope are meaningful, it requires calibrations as any other instrument. Calibration of x , y and z cartesian axis is done using standards that are verified by many other instruments, including the electron microscopes. To calibrate the electric potential measurements, a silicon wafer is oxidized forming a thin silica layer where a set of interdigitated electrodes made of evaporated gold is mounted, using microlithography techniques. The electrodes are connected to a precision DC voltage source and the potential on the electrodes is read using the Kelvin microscope set-up. During this calibration work, Rubia Gouveia noticed, in the author's laboratory, a pronounced effect of relative humidity shown in Fig. 6.11: the electric potential over silica is steady, under 10 or 30% but it changes pronouncedly with time, under 70%. Potential vs. time plots obtained during these experiments are shown in Fig. 6.12 [15].

The comparison of results obtained using the same protocol but under 10 or 70% relative humidity show marked differences and many intriguing points that were discussed in the paper. Most relevant to the present discussion is the pronounced difference between the potential vs. time plots for the silica surfaces, that was interpreted using the mechanism schematically depicted in Fig. 6.13. Electrode bias produces fast changes within times well-below 1 s followed by slow changes extending for many minutes.

Potential vs. distance plots were also acquired after the electrodes were short-circuited and grounded, at each RH. These are shown in Fig. 6.13, and they are also strongly dependent on the relative humidity. Line-scans measured at 70 and 50% RH show local potentials down to -1.2 V over silica and up to 0.3 V at the metal borders, forming regular, persistent patterns. The curves recorded under low RH also show deviations from zero but much smaller. This confirms that fixed charges are produced on silica while the electrodes are biased, and this is increasingly more pronounced at high RH.

All these observations are explained assuming the model presented in Fig. 6.14. Steep potential changes are observed following electrode connection to the power supply, followed by the formation of excess negative ion concentration in the surrounding atmosphere followed by the events described in the caption of Fig. 6.14.

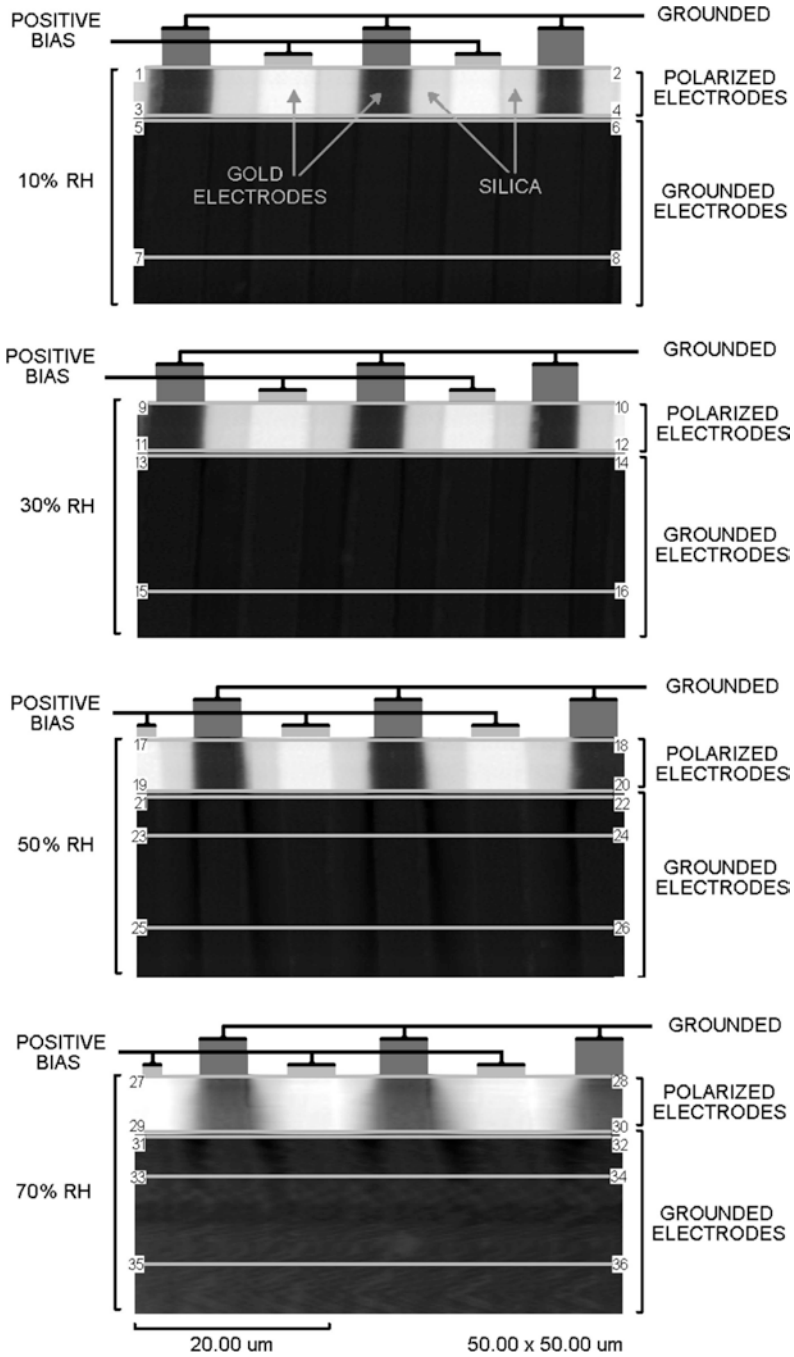


Fig. 6.11 KFM micrograph of a silica-on-wafer thin film partially covered with interdigitated electrodes. Successive changes in the state of electrode polarization and relative humidity of the surrounding atmosphere were made while the image was acquired, as indicated at the sides of the figures. Brighter areas are positive; dark areas are negative. Reprinted with permission from [15]

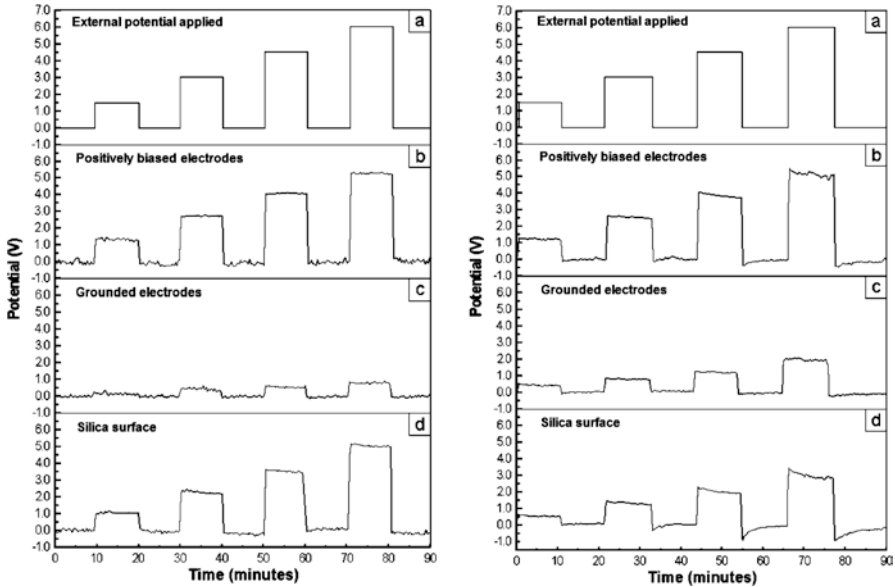


Fig. 6.12 (a) Potential difference applied to the metal electrodes. (b) Measured KFM potential over the biased electrode surface. (c) Measured potential over the grounded electrode. (d) Measured potential over the silica insulator in between the two electrodes. *Left:* 10% relative humidity. *Right:* 70% relative humidity. Reprinted with permission from [15]

6.4.3 Excess Charge Decay Through the Atmosphere

Water is usually seen as a passive agent for charge dissipation due to its low (but non-zero) electrical conductivity, following, for instance, the conclusions of Erwin Schrödinger's doctoral thesis [16]. It follows that charge elimination by surface conductance is the most often used mechanism for explaining the spontaneous decrease of charge under high humidity.

Saever [17] did detailed examination of this subject, in an attempt to explain the discrepancies reported in the literature, concluding that the surface resistivity of insulators is a measure of the amount of adsorbed water. Consequently, the relative humidity, temperature and the adsorption equilibrium of oxide pollutants and salts in the local atmosphere are all relevant variables responsible for the disparity in results obtained in different laboratories. It is important to keep in mind that surface water films are often discontinuous, due to dewetting phenomena [18, 19].

The role of the atmosphere as a source and sink of ions that was introduced in Sect. 6.2 contributes another path for charge transfer coupled to adsorption and desorption of H^+ and OH^- bound to water molecule clusters. Direct verification of the effectiveness of charge transfer to the atmosphere was obtained by following the discharge of corona- and tribocharged materials as a function of time and relative humidity. Quadruplicate samples were charged and allowed to discharge under

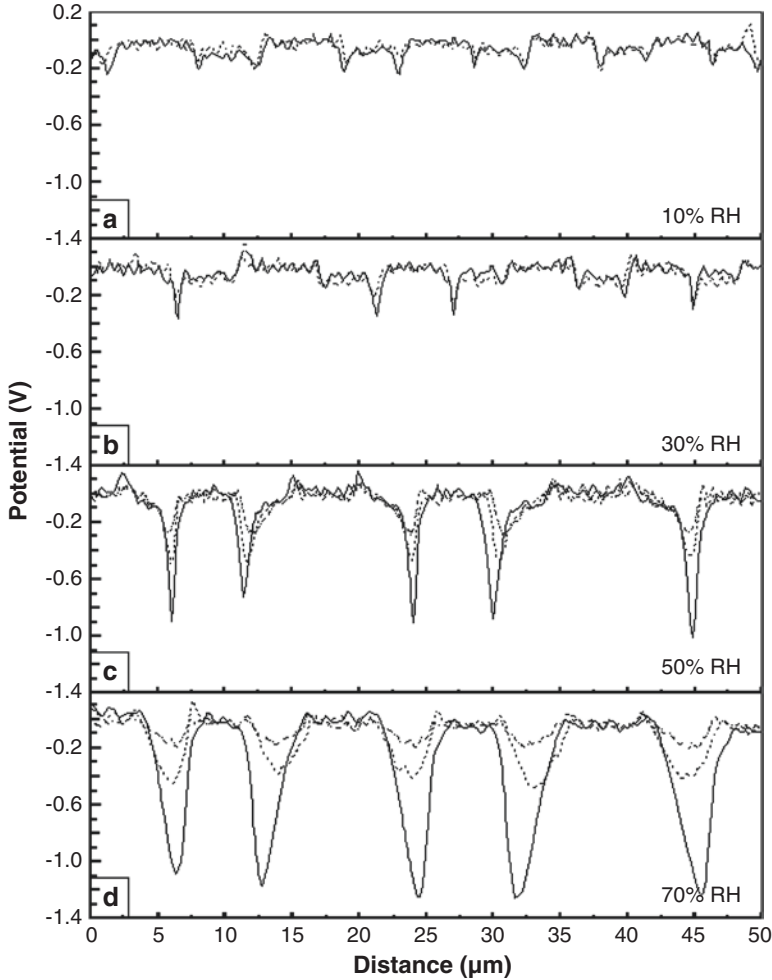


Fig. 6.13 Potential vs. distance along horizontal lines drawn in Fig. 6.11. *Solid line*: profiles acquired immediately after electrodes were grounded. *Dash line*: profiles acquired 10 min after electrodes grounding. *Dash dot line*: profiles acquired 30 min after electrodes grounding. (a) Profiles 5,6 (*solid line*) and 7,8 (*dash line*); (b) profiles 13,14 (*solid line*) and 15,16 (*dash line*); (c) profiles 21,22 (*solid line*), 23,24 (*dash line*) and 25,26 (*dash dot line*) and (d) profiles 31,32 (*solid line*) and 33,34 (*dash line*) and 35,36 (*dash dot line*), under 10, 30, 50, and 70% RH, respectively. Reprinted with permission from [15]

controlled relative humidity, while potential maps were recorded using a scanning Kelvin electrode, yielding potential half-lives.

Recorded curves for adjacent areas are uncorrelated, showing that charge surface motion is not the dominating mechanism for discharge. Relevant data are in Fig. 6.15. It shows half-lives of electric potential as a function of position for LDPE samples previously charged with positive and negative corona [20]. There are

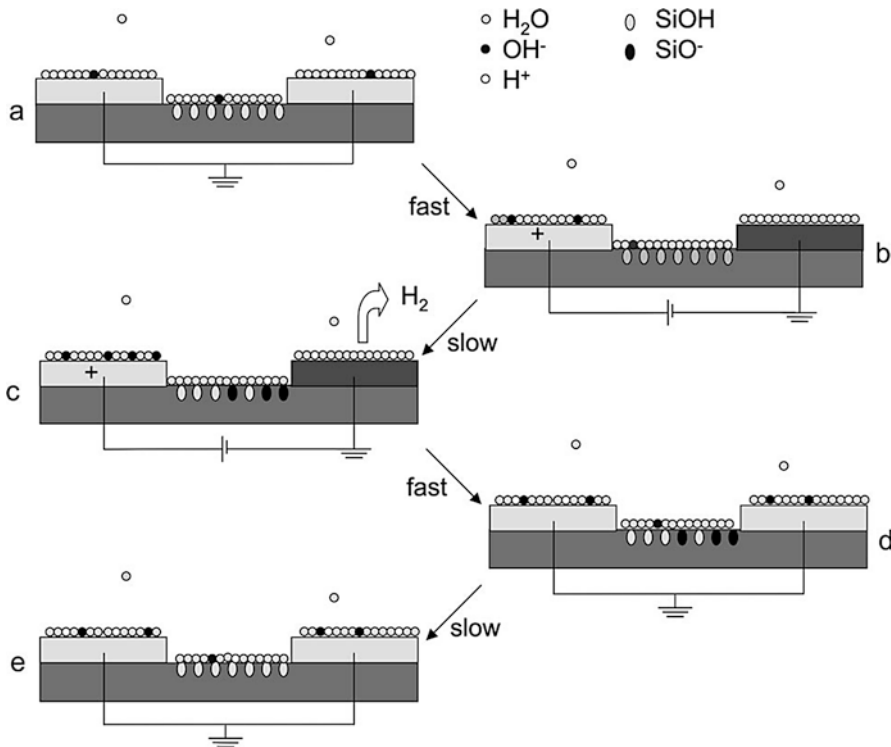


Fig. 6.14 Schematic representation of the model for the behavior of water molecule in the electrodes and silica surface, as well as of the silanol groups on silica. (a) In the initial state, the water film is neutral. At the gas–solid interfaces, (b) when an electrode set is biased, surface ions migrate to electrodes carrying potential of opposite signal; (c) silanol groups are slowly converted to silicate while H⁺ ions are discharged at the grounded electrode; (d) when the electrodes are all grounded, ions at the surface film migrate reforming a neutral water layer; (e) silicate groups bind H⁺ ions from water layer; (e) silicate groups bind H⁺ ions from water and they are thus neutralized. Reprinted with permission from [15]

significant differences between potential half-lives within any given sample, they are shorter for negative samples and highly dependent on the relative humidity.

An unexpected finding was that all the potential vs. time curves converge to low negative values (-4.6 ± 0.7 V). This non-dissipated potential was then called *equilibrium potential* [20] and it was observed for other hydrophobic polymers.

The following mechanism is consistent with these results:

1. OH⁻ ions from the vapor bind to surface sites S_{OH} on LDPE with rate $v_{dp} = [\text{OH}^-]_v [\text{S}_{\text{OH}}]$.
2. H⁺ ions from the vapor bind to surface sites S_{OH} on LDPE with rate $v_{dn} = [\text{H}^+]_v [\text{S}_{\text{H}}]$.

Since $v_{dp} > v_{dn}$, $K = v_{dp}/v_{dn} = [\text{S}_{\text{OH}}]/[\text{S}_{\text{H}}] > 1$, provided the $[\text{OH}^-]_v/[\text{H}^+]_v$ ratio is approximately equal to 1. This assumption is consistent with the symmetry for formation of positive and negative ions from water that was observed in other sections in this chapter.

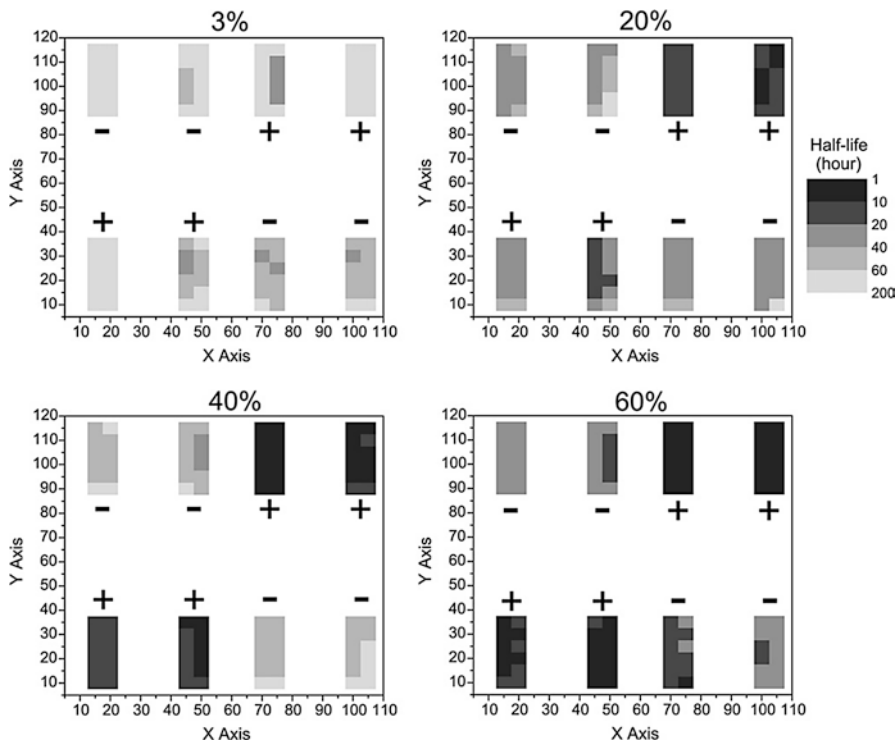


Fig. 6.15 Maps showing the half-lives of electric potential decay as a function of the position on LDPE pieces under variable relative humidity. Reprinted with permission from [20]

This mechanism explains all the experimental observations made in this experiment, placing it within a simple conceptual framework that is familiar even to high-school students. Moreover, it is consistent with the idea of specific OH^- adsorption on hydrophobic surfaces [21, 22].

The importance of surface conduction as the prevalent mechanism for discharge is also dismissed by experimental results on the discharge of tribocharged materials. The successive potential maps recorded on rubbed PTFE (see Fig. 6.16) show faster decay of positive pixels and no indication of charge neutralization at the separation between positive and negative areas [23].

6.5 Flow Electrification: The Position of Water in the Triboelectric Series

Liquid charging during flow within a pipe is well known as *flow electrification (FE)* that is a known oil pipeline hazard. It was also recently observed for many other liquids, including water. For instance, ultrapure water used in the fabrication of semiconductor chips can cause electrostatic discharges in electronic components

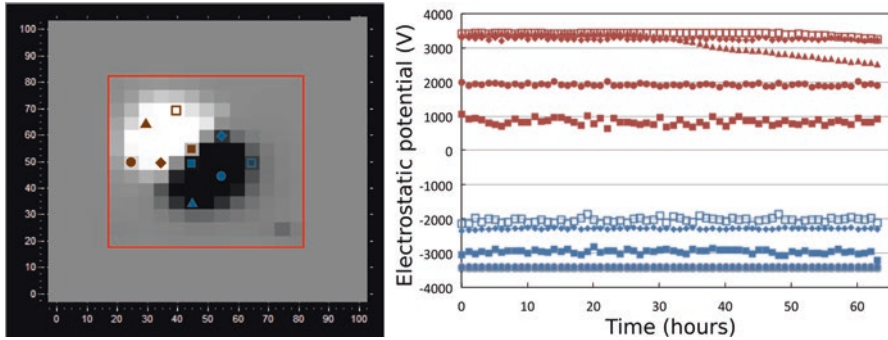


Fig. 6.16 Electrostatic potential variation on PTFE tribocharged with PE foam. (*Left*) Potential map of PTFE abraded with PE foam. (*Right*) Electrostatic potential of the selected pixels measured during 63 h at 60% relative humidity. Reprinted with permission from [23]

[24]. Other reports show that pure water flowing through hydrophobic materials such as polytetrafluorethylene (PTFE) becomes positively charged [25, 26]. However, there is only limited information on flow electrification of water with different surfaces [27].

A simple and robust apparatus provided reproducible results on excess electric charge acquired by water flowing through different materials [28]. The experimental setup is in Fig. 6.17a and a summary of results is presented in Fig. 6.17b. Water acquires a net positive charge against all solids tested and the charge magnitude follows most triboelectric series [29]. Acquisition of excess positive charge in water may be understood as a case of electrosmosis that is explained considering the preferential adsorption of OH^- ions at the solid surfaces. This produces an electric double layer with negative ions trapped at the Stern layer while the positive H^+ ions in the diffuse layer move with bulk water. This is represented in Fig. 6.17c.

This may also be related to the exclusion-zone formed on the vicinity of various hydrophilic surfaces [30, 31] that displays a negative net charge.

A recent report shows that water collected from various different places and placed within common containers (e.g. polyallomer centrifuge tube) is always negatively charged [32], in apparent disagreement with the results in Fig. 6.17. However, these measurements were made using a Faraday cup containing the whole system, water plus its recipient, not just water itself.

6.6 Water Dropping from a Biased Needle

Water with excess charge is obtained by connecting to a biased electrode and it can be stored in a Faraday cup [33].

Water dropping from an electrically biased needle acquires excess charge as shown in Fig. 6.18a. The charge sign is the same as the sign of the needle potential and it modifies the water surface tension, decreasing it pronouncedly, as in Fig. 6.18b.

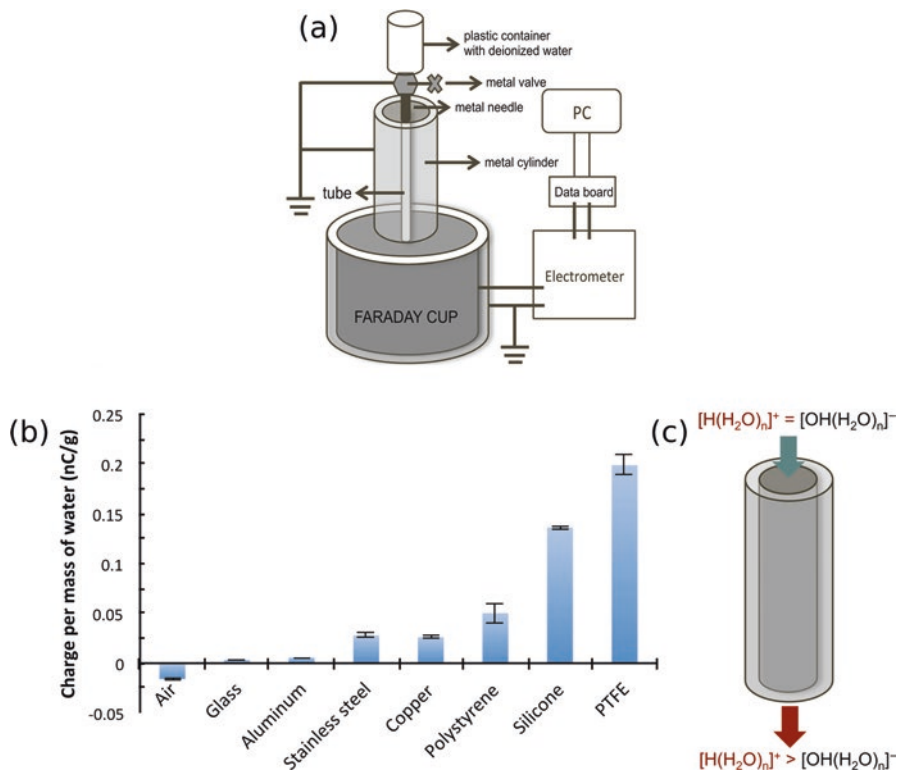


Fig. 6.17 (a) Experimental setup used to measure electric charge of water acquired by flowing through different materials; (b) Charge per unit weight of water following contact with different materials; (c) Schematic charging mechanism: neutral water enters the tubing where OH^- ions are adsorbed while H^+ ions remain within water. Reprinted with permission from [28]

This was verified by using the drop shape and drop volume/weight measurement techniques. The drops are distorted as the potential increases until the drops stretch into streaks of electrified liquid, at $V > 9$ kV, showing that electrostatic repulsion overcomes surface tension. Under high tension, sessile water drops resting on top of biased needles undergo Columbic explosion, sending smaller droplets upward.

Measuring charge, potential and surface tension of the electrified liquid provides all the information usually obtained from electrocapillarity experiments. This has been a limited topic of study due to the scarcity of conducting non-reactive liquids that made electrocapillarity virtually exclusive to the mercury electrodes that are not popular due to toxicity and environmental problems. However, the experimental protocols used by Santos et al. [33] are adaptable to most common liquids at room temperature and this brings feasibility to the study of electrocapillarity. One important outcome of these experiments is the demonstration that potential drop at the water–air interface is a few tens of volts only, when the water drop is biased in the kV region. This is the first estimate of potential drop within the electric double layer

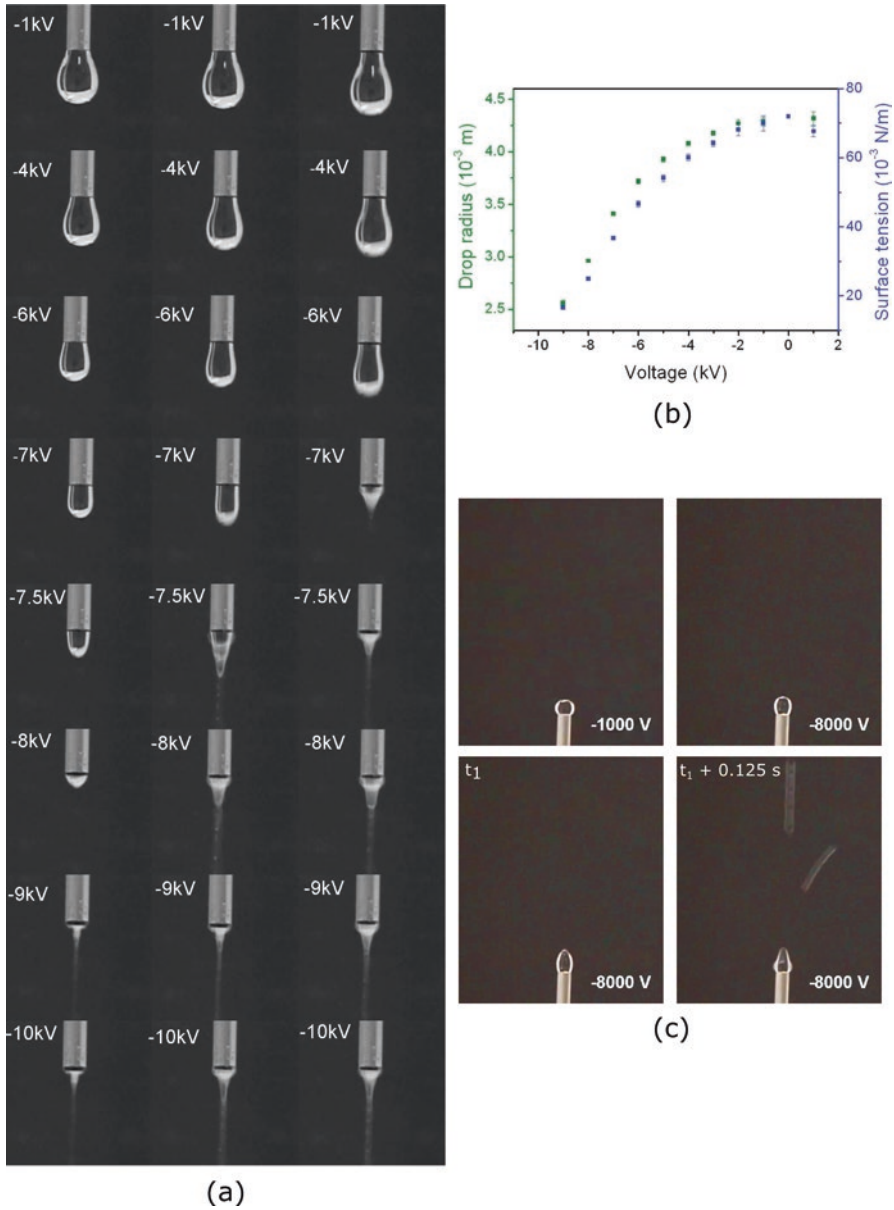


Fig. 6.18 (a) Water exiting the tip of a biased needle, showing Taylor cone formation, drop elongation, and Coulombic explosion at high V . Water flow: 64.1 mL/h. Distance from needle tip to the nearest grounded surface was ~ 10 cm. Pictures were chosen from a recorded video to represent interesting features, and time interval between them is not uniform; (b) Drop radius and calculated surface tension as a function of needle electric potential. Error bars are always plotted, but in some points they are smaller than the symbol. Minimum distance between needle tip and surrounding grounded surfaces was 1.1 m, to minimize electric field strength; (c) Coulombic explosion of a water sessile drop when the supporting needle is biased to -8000 V. Notice the faint streak on top of the photo. Parts of this figure are reprinted with permission from [33]

at a gas/liquid interface, ever. On the other hand, water density and viscosity are unaltered, showing that charges are accumulated at interfaces only and do not affect bulk properties.

6.7 Spontaneous Electric-Bipolar Nature of Aerosols

Aerosols are widely found on the Earth's atmosphere and have paramount importance in atmospheric phenomena [34], including a large number of chemicals discharged in the atmosphere by natural and anthropic phenomena. Aqueous aerosols are particularly relevant for cloud formation, stability and rain precipitation, while clouds are also important as precursors of atmospheric aerosols formed by other chemical substances [35, 36]. Many authors in this area relate atmospheric electricity to liquid water or ice particles and assign its formation to ice particle breakdown within storm clouds, while others give great importance to air ionization due to radiation.

Aerosol formation, properties and stability are often related to important practical problems in industrial, energy and health contexts. For this reason, there is excellent information on charge in aerosols [37] but this is not shown in the literature in atmospheric chemistry, as frequently as in the literature on colloidal sols, where zeta potentials or particle charge data appear in nearly every paper.

A robust and reproducible method to generate a current of aerosol is a nebulizer used for domestic inhalation. Charge in aerosol is detected by targeting the flowing aerosol to the interior of a Faraday cup while simultaneously measuring the electrostatic potential of the nebulizer with residual water, using a macroscopic Kelvin electrode [38], as shown in Fig. 6.19a. Moreover, aerosol electrophoresis is done by passing the aerosol in between two parallel copper disks connected to a high voltage power supply, as in Fig. 6.19b. These two procedures do not give detailed information on particle size and charge distribution but they yield information on particles as they leave the aerosol source, with minimal particle manipulation [39].

When aerosol from deionized water stemming out of a nebulizer passes through the inner electrode of the Faraday cup it produces initially highly variable positive current (Fig. 6.20a), changing to a time series of sharp positive and negative current peaks. When the aerosol is made using an aqueous NaCl solution, a similar result is obtained but the initial current is negative (Fig. 6.20b). The positive and negative peaks show that the aerosol is bipolar, this means, it contain both positive and negative droplets.

Observation of aerosol motion within an electric field confirms the bipolar charging behavior: when the aerosol enters the inter-electrode volume, it divides into convective streaks that migrate separately toward each electrode. Some suggestive frames are shown in Fig. 6.21. In control runs, aerosol flows undistorted in between grounded electrodes. Aerosol from deionized water deviates largely toward the negative electrode but a significant amount migrates to the positive electrode. Aerosol from NaCl solution also deviates, but the bulkier stream moves toward the positive pole.

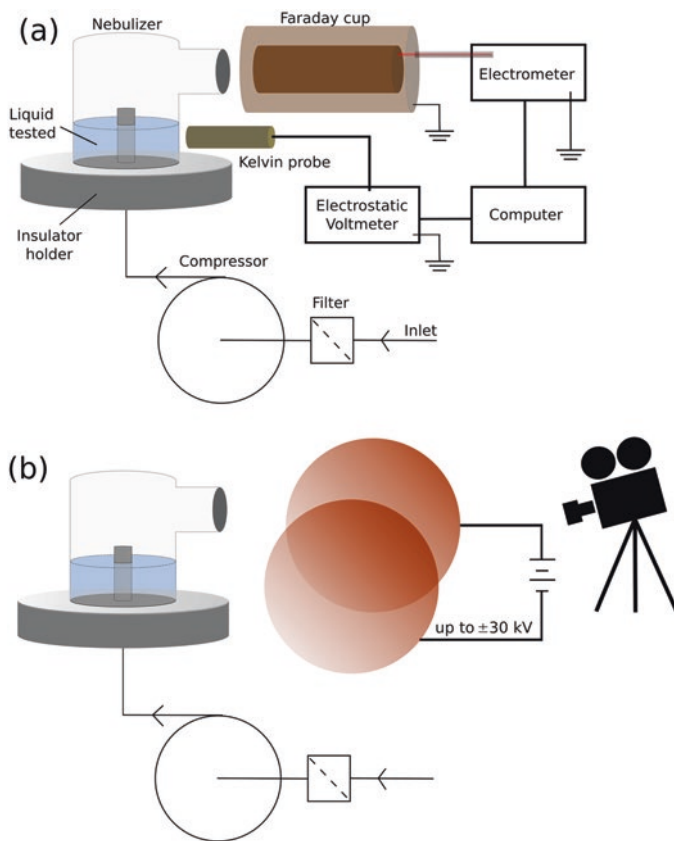


Fig. 6.19 Setups to measure aerosol charging and electrophoresis. Reprinted with permission from [39]

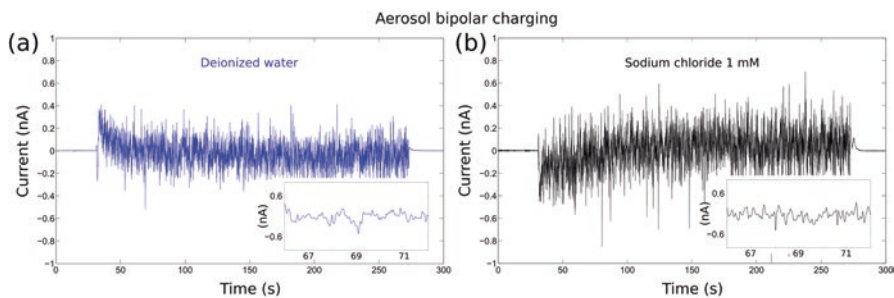


Fig. 6.20 Electric current between the electrodes of a Faraday cup, produced by passing aerosol from (a) deionized water and (b) sodium chloride solution (1 mmol L^{-1}) measured at a high-speed acquisition rate (800 readings/s). Reprinted with permission from [39]

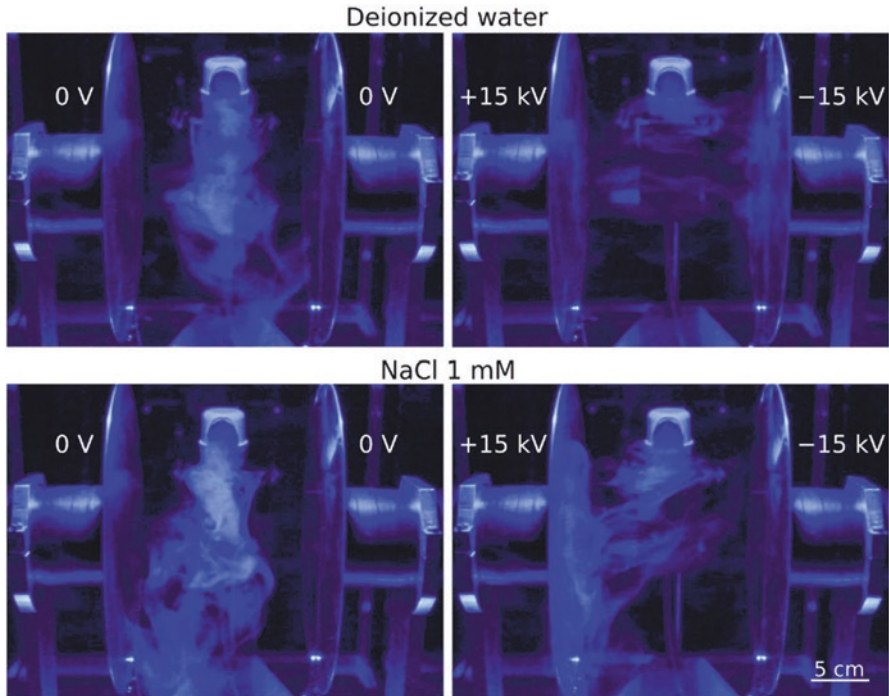


Fig. 6.21 Aerosol electrophoresis. Liquid is deposited on both electrodes, revealing that both positive and negatively charged droplets coexist in the aerosol. Reprinted with permission from [39]

These results show that liquid fragmentation by dropping, splashing and other frequent phenomena introduces electrostatic charge into the environment, where it is absorbed or adsorbed in the surrounding objects. This shows that the atmosphere is always filled with ions derived from water, salt and other common substances. For this reason, the often-quoted ionization caused by high-energy particles crossing the atmosphere is not essential for the appearance of atmospheric electricity [38, 39], even though it certainly makes a contribution.

The new understanding on charge bipolarity in aerosols may contribute to progress in scavenging electrical energy from the atmosphere and to increase safety while handling liquids in industrial environments. Finally, enlarging current knowledge on aerosol charging phenomena and mechanisms will probably contribute to a better understanding of atmospheric charge formation and stability.

6.8 Conclusion and Prospects

Water plays a dual role in electrostatic phenomena. It contributes to discharging by surface and bulk conduction thanks to the mobility of its ions, $\text{H}(\text{H}_2\text{O})_n^+$ and $\text{OH}(\text{H}_2\text{O})_n^-$ but it also plays the opposite role, acting an electrifying agent through

different processes: adsorption of vapor on metals and insulators and partition during phase transition. Given its ability to partition and transfer ionic charge, water can also store charge reaching high potential. This has not yet been exploited for charge storage but the possibility is obvious with the perspective of achieving high energy density.

The electrification processes cover quite different potential ranges, from a few hundreds of millivolts to thousands of volts. Most relevant, charge transfer associated with mass transfer has a unique feature: it depends on the geometrical distribution of charge. This means, if a set of particles is charged to a given potential and then particles are brought to close proximity while maintaining their individual charges, the potential reached by the particle assembly will largely exceed the charging potential. This is at the core of functioning of the Pelletron high voltage machines but it is probably also related to the creation of hazardous conditions in handling powders and liquids.

References

1. Agam N, Berliner PR (2006) Dew formation and water vapor adsorption in semi-arid environments—a review. *J Arid Environ* 64:572–590
2. Ludwig R (2001) Water: from clusters to the bulk. *Angew Chem Int Ed* 40:1808–1827
3. Hagymassy J, Brunauer S et al (1969) Pore structure analysis by water vapor adsorption. *J Colloid Interf Sci* 29:485–491
4. Hutson ND, Yang RT (1997) Theoretical basis for the Dubinin-Radushkevitch (D-R) adsorption isotherm equation. *Adsorption* 3:189–195
5. Solomon I, Ribeiro AM et al (2013) Adsorption equilibrium of water vapor on activated carbon and alumina and carbon and alumina impregnated with hygroscopic salt. *Turk J Chem* 37:358–365
6. Homma Y, Chiashi S et al (2013) Photoluminescence measurements and molecular dynamics simulations of water adsorption on the hydrophobic surface of a carbon nanotube in water vapor. *Phys Rev Lett* 110:157402
7. Soares LC, Bertazzo S et al (2008) A new mechanism for the electrostatic charge build-up and dissipation in dielectrics. *J Brazil Chem Soc* 19(2):277–286
8. Ducati TRD, Simões LH et al (2010) Charge partitioning at gas-solid interfaces: humidity causes electricity buildup on metals. *Lagmuir* 26(17):13763–13766
9. Danaa CDP, Banazakia AS et al (2015) Humidity potential as hygroelectric power in Indonesia: opportunities and challenges. In: *The 4th Indonesia EBTKE-ConEx, Jakarta*, pp 127–130
10. Gouveia RF, Galebeck F (2009) Electrostatic charging of hydrophilic particles due to water adsorption. *J Am Chem Soc* 131:11381–11386
11. Gouveia RF, Bernardes JS et al (2012) Acid-base site detection and mapping on solid surfaces by Kelvin force microscopy (KFM). *Anal Chem* 84:10191–10198
12. Tanabe K, Misono M et al (eds) (1989) *New solid acids and bases: their catalytic properties*. In: *Studies in surface science and catalysis*, vol 51. Elsevier Science, New York
13. Barth C, Foster AS et al (2011) Recent trends in surface characterization and chemistry with high-resolution scanning force methods. *Adv Mater* 23:477–501
14. Janzen MC, Ponder JB et al (2006) Colorimetric sensor arrays for volatile organic compounds. *Anal Chem* 78:3591–3600
15. Gouveia RF, Costa CAR et al (2008) Water vapor adsorption effect on silica surface electrostatic patterning. *J Phys Chem C* 112:17193–17199

16. Schrödinger E (1910) Über die Leitung der Elektrizität auf der Oberfläche von Isolatoren an feuchter Luft. Ph.D. thesis, University of Wien
17. Seaver AE (2005) Surface resistivity of uncoated insulators. *J Electrocardiol* 63:203–222
18. Lee LT, Leite CAP et al (2004) Controlled nanoparticle assembly by dewetting of charged polymer solutions. *Langmuir* 20:4430
19. Bernardes JS, Rezende CA et al (2010) Morphology and self-arraying of SDS and DTAB dried on mica surface. *Langmuir* 26:7824–7832
20. Burgo TAL, Rezende CA et al (2011) Electric potential decay on polyethylene: role of atmospheric water on electric charge build-up and dissipation. *J Electrostat* 69:401–409
21. Healy TW, Fuerstenau DW (2007) The isoelectric point/point-of zero-charge of interfaces formed by aqueous solutions and nonpolar solids, liquids, and gases. *J Colloid Interf Sci* 309:183–188
22. Kudin KN, Car R (2008) Why are water-hydrophobic interfaces charged? *J Am Chem Soc* 130:3915–3919
23. Burgo TAL, Ducati TRD et al (2012) Triboelectricity: macroscopic charge patterns formed by self-arraying ions on polymer surfaces. *Langmuir* 28:7407–7416
24. Yatsuzuka K, Mizuno Y et al (1994) Electrification phenomena of pure water droplets dripping and sliding on a polymer surface. *J Electrostat* 32:157–171
25. Yatsuzuka K, Higashiyama Y et al (1996) Electrification of polymer surface caused by sliding ultrapure water. *IEEE Trans Ind* 32:825–831
26. Ravelo B, Duval F et al (2011) Demonstration of the triboelectricity effect by the flow of liquid water in the insulating pipe. *J Electrostat* 69:473–478
27. Paillat T, Moreau E et al (2000) Streaming electrification of a dielectric liquid through a glass capillary. In: *Industry Applications Conference, 2000, Conference Record of the 2000 IEEE*, vol 2, pp 743–748
28. Burgo TAL, Galembeck F et al (2016) Where is water in the triboelectric series? *J Electrostat* 80:30–33
29. Diaz AF, Felix-Navarro RM (2004) A semi-quantitative tribo-electric series for polymeric materials: the influence of chemical structure and properties. *J Electrostat* 62:277–290
30. Zheng JM, Chin W et al (2006) Surfaces and interfacial water: evidence that hydrophilic surfaces have long-range impact. *Adv Colloid Interf Sci* 127:19–27
31. Das R, Pollack GH (2013) Charge-based forces at the Nafion-water interface. *Langmuir* 29:2651–2658
32. Amin MS, Peterson TF Jr et al (2006) Advanced Faraday cage measurements of charge and open-circuit voltage using water dielectrics. *J Electrostat* 64:424–430
33. Santos LP, Ducati TRD et al (2011) Water with excess electric charge. *J Phys Chem* 115:11226–11232
34. Kaufman YJ, Tanré D et al (2002) A satellite view of aerosols in the climate system. *Nature* 419:215–223
35. Hirsikko A, Nieminen T et al (2011) Atmospheric ions and nucleation: a review of observations. *Atmos Chem Phys* 11:767–798
36. Zhang R, Khalizov A et al (2012) Nucleation and growth of nanoparticles in the atmosphere. *Chem Rev* 112:1957–2011
37. Wong J, Knok PCL et al (2016) Bipolar electrostatic charge and mass distributions of powder aerosols—effects of inhaler design and inhaler material. *J Aerosol Sci* 95:104–117
38. Burgo TAL, Galembeck F (2016) Electrified water: liquid, vapor and aerosol. *J Brazil Chem Soc* 27:229–238
39. Burgo TAL, Galembeck F (2015) On the spontaneous electric-bipolar nature of aerosols formed by mechanical disruption of liquids. *Colloids Interf Sci Commun* 7:7–11